Journal of Medicinal Chemistry

Article

Development of a potent wound healing agent based on the liver fluke granulin structural fold.

Paramjit S. Bansal, Michael J. Smout, David Wilson, Claudia Cobos Caceres, Mohadeseh Dastpeyman, Javier Sotillo, Julia Seifert, Paul J. Brindley, Alex Loukas, and Norelle L. Daly

J. Med. Chem., **Just Accepted Manuscript** • Publication Date (Web): 20 Apr 2017

Development of a potent wound healing agent based on the liver fluke granulin structural fold

Paramjit S. Bansal[1#], Michael J. Smout[1#], David Wilson[1], Claudia Cobos Caceres[1], Mohadeseh Dastpeyman[1], Javier Sotillo[1], Julia Seifert[1], Paul J. Brindley[2], Alex Loukas[1*], Norelle L. Daly[1*]

[1]Centre for Biodiscovery and Molecular Development of Therapeutics, Australian Institute of Tropical Health and Medicine, James Cook University, Cairns, QLD Australia. [2]Department of Microbiology, Immunology and Tropical Medicine, and Research Center for Neglected Diseases of Poverty, School of Medicine & Health Sciences, George Washington University, Washington DC, U.S.A.

[#]These authors contributed equally to this research. [*]To whom correspondence should be addressed:

Professor Norelle L. Daly

Address: Centre for Biodiscovery and Molecular Development of Therapeutics, AITHM, James Cook University, QLD 4870, Australia

Email: norelle.daly@jcu.edu.au

Phone: +61-7-4232 1815

Professor Alex Loukas

Address: Centre for Biodiscovery and Molecular Development of Therapeutics, AITHM, James Cook University, QLD 4870, Australia

Email: alex.loukas@jcu.edu.au

Phone: +61-7-4232 1608

Abstract

Granulins are a family of protein growth factors that are involved in cell proliferation. An orthologue of granulin from the human parasitic liver fluke *Opisthorchis viverrini*, known as *Ov*-GRN-1, induces angiogenesis and accelerates wound repair. Recombinant *Ov*-GRN-1 production is complex, and poses an obstacle for clinical development. To identify the bioactive region(s) of *Ov*-GRN-1, four truncated N-terminal analogues were synthesized and characterized structurally using NMR spectroscopy. Peptides that contained only two native disulfide bonds lack the characteristic granulin β-hairpin structure. Remarkably, the introduction of a non-native disulfide bond was critical for formation of β-hairpin structure. Despite this structural difference, both two and three disulfide-bonded peptides drove proliferation of a human cholangiocyte cell line and demonstrated potent wound healing in mice. Peptides derived from *Ov*-GRN-1 are leads for novel wound healing therapeutics, as they are likely less immunogenic than the full-length protein and more convenient to produce.

Introduction

Granulins are a family of protein growth factors involved in a wide range of physiological functions and disease processes including embryogenesis, wound repair, inflammation and tumour growth[1]. The human parasitic liver fluke *Opisthorchis viverrini* secretes a granulin family member called *Ov*-GRN-1, which was originally isolated from the excretory/secretory (ES) products of the carcinogenic trematode[2, 3]. *Ov*-GRN-1 was the first growth factor described from a pathogen to cause proliferation of both human and murine cells[4, 5]. We have shown that picomolar concentrations of recombinant *Ov*-GRN-1 induce angiogenesis and accelerate wound repair in mice upon topical administration, findings that indicate that liver fluke granulin might be developed as a treatment for wounds[6].

An understanding of the structure-activity relationship for *Ov*-GRN-1 would enable design of the most efficacious form of this granulin for healing wounds. The three-dimensional structure of *Ov*-GRN-1 has not been experimentally determined, but structures for granulins of several species have been reported. The initial granulin structure determined was that of carp granulin-1; this comprises four β-hairpins cross-linked together by six disulfide bonds in a ladder-shaped arrangement of the disulfide bonds[7]. Despite the well-defined structure observed for carp granulin-1, the structure function relationships of granulins are complex and appear to be highly dependent on the primary sequence. This is particularly evident with the human granulins. The precursor protein of mammalian granulin (progranulin, PGRN) contains seven-and-a-half granulin domains that are approximately 6 kDa in molecular mass and are proteolytically

processed into individual granulin modules after secretion of PGRN from the cell[1]. The "half-granulin" unit, termed paragranulin, contains only six cysteine residues[8].

The seven human granulin modules have been expressed individually and the structures analyzed by NMR spectroscopy[9]. Three contain relatively well-defined three-dimensional structures in solution (A, C and F), whereas the others are mainly mixtures of poorly structured disulfide isomers[9]. The structure of human granulin A includes a β-hairpin structure similar to carp granulin-1 but there is significant structural disorder in the C-terminal region. Of the well folded human granulin modules, granulin A demonstrates potent inhibition of proliferation of a breast cancer cell line, while by contrast, human granulin F stimulates cell proliferation[9]. The poorly folded peptides exhibit weak or no inhibitory or activity. It should be noted, however, that the limited activity may be due to the absence of key signaling pathways in the target cells, and/or that the production of the recombinant peptides in bacteria induced incomplete/incorrect folding. To date, the range of granulin activities and binding partners is broad, and seemingly organ- and co-factor-dependent[10-13].

Structural analysis with NMR spectroscopy has shown that the N-terminal regions of carp granulin-1 and human granulin A can fold independently of the C-terminal regions[14, 15]. Truncated analogues of these two granulins containing only two-disulfide bonds, have β-hairpin structures, as shown for a 30-residue N-terminal domain of carp granulin-1 (Figure 1). In the current study we synthesized truncated versions of *Ov*-GRN-1 to determine if this region can fold independently, and to determine if the N-terminal region contributes to cell proliferation and wound healing. We show for the first time that the N-terminal region of *Ov*-GRN-1 displays

novel folding properties, and notably from a drug design perspective, peptides derived from the N-terminus are as potent as the full-length protein and Regranex, a clinically used wound-healing agent, in healing cutaneous wounds in laboratory mice.

Results

Design and synthesis of truncated Ov-GRN-1 peptides

To determine if the N-terminal region of *Ov*-GRN-1 can fold independently several truncated peptides were designed and synthesized using FMOC chemistry. The sequences of the synthetic peptides are shown in Figure 2A.

Ov-GRN$_{1-35}$, *Ov*-GRN$_{8-38}$ and *Ov*-GRN$_{12-34}$ all contain four cysteine residues equivalent to Cys I, Cys II, Cys III and Cys V in the full length protein (for the remainder of the report, Roman numerals refer to the numbering present in the full length protein). Cys IV and Cys VI were predicted to form disulfide bonds with Cys VII and Cys IX respectively, based on the three-dimensional structure of carp granulin-1[7]. In the truncated analogues Cys IV and Cys VI were replaced with alanine residues to prevent disulfide bond formation between these residues. Selective protection of the cysteine residues was used to direct the folding to form the predicted disulfide connectivity (i.e. Cys I-Cys III and Cys II-Cys V).

Ov-GRN-1 contains an extended N-terminal tail (11 residues prior to the first cysteine residue) not present in the majority of granulins, and these residues were included in *Ov*-GRN$_{1-35}$ to determine if they play a role in the bioactivity. The N-terminus was truncated and the C-terminus extended in *Ov*-GRN$_{8-38}$ to provide an analogue with a similar number of residues to the carp granulin-1 truncated peptide. *Ov*-GRN$_{12-34}$ is the minimal sequence that contains the four cysteine residues (CysI, CysII, CysIII and CysV) and was designed to determine if the N- and C-terminal regions are required for folding and activity.

An additional peptide was synthesised (*Ov*-GRN$_{12\text{-}35_3s}$) with a truncated N-terminus but containing the first six cysteines of *Ov*-GRN-1 (the "3s" refers to the presence of three-disulfide bonds in the peptide). This peptide is analogous to mammalian paragranulin (above) in terms of the cysteine residues. It was synthesized without selective protection of the cysteine residues and the major conformation was purified for analysis of its structure and activity.

Structural analysis with NMR spectroscopy

NMR spectroscopy was employed to analyse the structure of the peptides. The one-dimensional spectra of *Ov*-GRN$_{1\text{-}35}$, *Ov*-GRN$_{8\text{-}38}$ and *Ov*-GRN$_{12\text{-}34}$ have limited dispersion in the amide regions consistent with a lack of β-sheet structures despite formation of the two native disulfide bonds. Two-dimensional spectra (TOCSY and NOESY) were used to assign the resonances, and the secondary shifts were determined by subtracting random coil shifts[16] from the αH shifts. The secondary shifts are similar over the equivalent residues for these three peptides, as shown in Figure 2B, indicating that the structures were similar and consequently, that the differences in the N- and C-termini of these peptides did not influence the overall fold. Furthermore, the secondary shifts were consistent with a lack of β-sheet structure as they are primarily negative and β-sheet structures are characterised by positive secondary shifts. The three-dimensional structure of *Ov*-GRN$_{12\text{-}34}$ was determined using NMR spectroscopy, as shown in Figure 3A. In contrast to the characteristic granulin fold, the structure comprised turns and a region of 3_{10} helix. The structure statistics are provided in Supplementary Table S1.

In contrast to the two-disulfide bond-containing *Ov*-GRN-1 peptides, *Ov*-GRN$_{12\text{-}35_3s}$, with three-disulfide bonds has more dispersion in the amide region in the one-dimensional NMR spectrum.

Furthermore, additional peaks were present in the spectra, likely due to isomerisation of the proline residues. Despite these additional peaks, the major conformation was fully assigned, and the secondary shifts were similar to the truncated carp granulin-1[14] (Figure 3B), which indicates the similarity of the overall structures. Truncated carp granulin-1, comprising residues 1-30, has previously been synthesised with Cys IV and Cys VI replaced with serine residues, and was shown to form a β-sheet structure[14]. Here we synthesised carp granulin$_{1\text{-}30}$ with Cys IV and Cys VI replaced with alanine residues to be consistent with the truncated peptides of *Ov*-GRN-1. Only minor variations were evident between the published[14] chemical shifts of carp granulin-1 with the serine substitutions and the peptide with the alanine substitutions (Supplementary Figure S1), indicating that the overall fold is still maintained.

To confirm if the structure of *Ov*-GRN$_{12\text{-}35_3s}$ was similar to carp granulin$_{1\text{-}30}$, three-dimensional structures were calculated using CYANA. Structures were initially calculated without disulfide bond restraints. In these structures a β-hairpin was present from residues 14-23, but residues 1-8 were not defined. The lack of definition for residues 1-8 prevented an analysis of the sulfur-sulfur distances providing insight into the most likely connectivity. Therefore, an alternative approach was used whereby the structures were calculated with the 15 possible disulfide bond connectivities. This approach has previously been used for disulfide-rich peptides such as the cyclotides to analyse the disulfide bond connectivities[17, 18]. The CYANA target functions for the 15 connectivities for *Ov*-GRN$_{12\text{-}35_3s}$ are shown in Supplementary Table S2. The connectivity with the lowest CYANA target function was CysI-CysIII, CysII-CysV and CysIV-CysVI. The three-dimensional structure of *Ov*-GRN$_{12\text{-}35_3s}$ with this connectivity is shown in Figure 3A and the structure statistics provided in Supplementary Table S1. The most well defined region of the

molecule was the β-hairpin between residues 14-23. The N-terminal region, encompassing CysI and CysII displayed marked structural disorder.

Cell proliferation

The influence of the *Ov*-GRN-1 peptides on proliferation of H69 cholangiocytes in real time was assessed using xCELLigence technology and dose response curves were determined for the peptides. *Ov*-$GRN_{12\text{-}35\_3s}$ at a final concentration of 2 μM resulted in a 41% increase in cell growth compared to control peptide ($p<0.0001$) (Figure 4A). A dose response curve similar to that obtained for *Ov*-GRN-1 was observed with *Ov*-$GRN_{12\text{-}35\_3s}$ treatment, characterized by significantly increased cell proliferation at final concentrations of ≥15 nM ($p<0.05$). The two-disulfide bonded *Ov*-GRN-1 peptides were less potent at nanomolar concentrations, but at 2 μM promoted significant cell proliferation (14-25% above peptide control; $p<0.01$) with dose response curves typified by *Ov*-$GRN_{12\text{-}34}$ (Figure 4A). No cell cytotoxicity was observed for any of the peptides tested at concentrations up to 2 μM.

The cell proliferation observed for the *Ov*-GRN peptides is in contrast to carp $granulin_{1\text{-}30}$ that induced minimal cell proliferation (non-significant) at all concentrations tested, and maximum proliferation of 9% over peptide controls at 32 nM. The response at 400 nM of all the *Ov*-GRN peptides (Figure 4B) highlights the enhanced potency of the three-disulfide bonded peptide (*Ov*-$GRN_{12\text{-}35\_3s}$) compared to the two-disulfide bonded peptides. *Ov*-$GRN_{12\text{-}35\_3s}$ promoted a highly significant ($p<0.0001$) increase in cell proliferation (26% over peptide controls) compared to the remaining peptides that induced minimal proliferation, of which the most potent was *Ov*-$GRN_{1\text{-}35}$ (9% non-significant increase over peptide control).

Mouse wound healing model

The truncated *Ov*-GRN-1 peptides formulated with methylcellulose were tested in a mouse model of wound healing. All *Ov*-GRN-1 peptides exhibited potent activity (Figure 5A, B) when applied topically compared to control peptide in methycellulose. The *Ov*-GRN-1 peptides, *Ov*-GRN-1 protein and Regranex significantly improved healing compared to peptide control on days 2-4 ($p<0.05$). As wounds closed, differences among treatments waned and significant differences were unapparent beyond day 4. Regranex and the various granulin peptides showed near identical best-fit curves and intact *Ov*-GRN-1 was the only compound tested here that provided significant improvement over Regranex on days 3 and 4 ($p<0.05$; Figure 5B). Significant differences were not observed between the various negative control groups formulated with methylcellulose, including PBS vehicle control, peptide control, and thioredoxin (TRX) recombinant protein control.

When healing at day 4 (Figure 5C, Supplementary Figure S2) was evaluated relative to PBS vehicle from each biological replicate, treatment of wounds with *Ov*-GRN-1 protein and peptides significantly accelerated wound healing compared to controls ($p<0.01$ at day 4: 26-41% over PBS). Although the *Ov*-GRN-1 protein, *Ov*-GRN_{1-35} and *Ov*-GRN_{12-34} (37-41% over PBS) provided improved healing compared to Regranex (29% over PBS), none of these comparisons reached significance at the day 4 time point.

Discussion

Elucidating the structure/activity relationships of granulins has been challenging given the sequence and structural variations in this protein family. Regions with bioactivity are poorly understood, and uncertainty remains about potential receptors for this growth factor[19, 20].

Ov-GRN-1 appears to have distinct folding pathways compared to other granulins. The N-terminal region of *Ov*-GRN-1, comprising two native disulfide bonds (CysI-CysIII and CysII-V), does not fold independently into a native-like β-hairpin structure, in contrast to carp granulin-1 and human granulin A. It is noteworthy that the introduction of a third, non-native disulfide bond in *Ov*-$GRN_{12\text{-}35\_3s}$ results in a β-hairpin structure similar to that present in the carp granulin-1 and human granulin A peptides[14, 15]. The disulfide bond connectivity of *Ov*-$GRN_{12\text{-}35\_3s}$ appears to comprise the two native disulfide bonds (CysI-CysIII and Cys II-V) in addition to the CysIV-CysVI disulfide bond. If the bond pairs are conserved across species[7, 9], the latter bond is predicted not to be present in the full length *Ov*-GRN-1, as CysIV is predicted to bond to CysVII and CysVI to CysIX.

The paragranulin (half-granulin) domain of mammal progranulin contains the equivalent six cysteine residues present in *Ov*-$GRN_{12\text{-}35\_3s}$ and is biologically active[21], which suggests that *Ov*-$GRN_{12\text{-}35\_3s}$ potentially contains the same disulfide connectivity. Carp $granulin_{1\text{-}30}$ peptide might accommodate this CysI-CysIII, Cys II-CysV, CysIV-CysVI connectivity[14]. Although carp $granulin_{1\text{-}30}$ peptide contains only the two native disulfide bonds (CysI-CysIII and Cys II-CysV), analysis of the structure indicates that the side-chains of the serine residues, which replace CysIV

and CysVI, are in close proximity, and suggest that it is feasible for these cysteine residues to form a disulfide bond.

The disulfide connectivity in *Ov*-GRN$_{12\text{-}35_3s}$ has implications for the structure of full-length *Ov*-GRN-1, which has not been experimentally determined because sufficient quantities of correctly folded recombinant material remain unavailable. Therefore, the disulfide connectivity of the native protein has not been shown to conform to the connectivity originally shown for carp granulin-1[7]. It is conceivable that the protein contains a disulfide domain comprising the first six cysteine residues (equivalent to that seen in *Ov*-GRN$_{12\text{-}35_3s}$), and a second domain containing the last six cysteine residues. Without the structure of the full-length protein and a comparison to the native protein secreted by the parasite, this remains speculation. However, previous reports revealed ambiguity in the disulfide connectivity of granulins[9, 15]. The structures of human granulin A and F have well-defined N-terminal regions, but disordered C-terminal regions prevented characterisation of all the disulfide bonds. Furthermore, chemical analysis of the disulfide connectivity of human granulin A was inconclusive[9].

In addition to providing insight into the folding of *Ov*-GRN-1, the current study revealed that the N-terminal region contributes to the bioactivity and the β-hairpin of *Ov*-GRN$_{12\text{-}35_3s}$ further enhanced cell proliferation activity. However, the β-hairpin structure is far from the complete story in regard to proliferative activity, as the carp granulin$_{1\text{-}30}$ peptide contains dual β-hairpins and in contrast to the *Ov*-GRN-1 peptides, showed no substantial proliferation at the eight concentrations tested (10 nM - 2 μM). A comparison of the sequences of carp granulin-1 with *Ov*-GRN-1 reveals that there are only two conserved non-cysteine residues between CysI and

CysVI. This lack of conservation in the loop sequences likely accounts for the differences in both folding and bioactivity.

Despite the lack of native structure, the two-disulfide bond containing *Ov*-GRN-1 peptides promoted cell proliferation at high concentrations (>800 nM) and stimulated significant healing of cutaneous wounds in mice. *Ov*-$GRN_{12\text{-}35\_3s}$ was the most potent peptide in the cell proliferation assay, but was no more active *in vivo* than the other *Ov*-GRN-1 peptides. If the β-hairpin of *Ov*-$GRN_{12\text{-}35\_3s}$ is involved in wound healing *in vivo* we did not observe a difference in mice. Cell proliferation activity may be cell line-specific, or alternatively the concentrations tested in mouse wound repair were not optimal. In either case, the activity observed in mice may be of greater biological and therapeutic consequence than findings from the *in vitro* analysis. In the future, we envision exploring a range of cells from diverse organs and tissues and investigation of mice that exhibit deficits in wound healing in order to increase our understanding of the role of *Ov*-GRN-1 structure-activity relationships.

To conclude, structural analysis with NMR spectroscopy suggested that *Ov*-GRN-1 exhibits unique folding properties compared with other granulins, presumably resulting from primary sequence. We have identified a bioactive region of *Ov*-GRN-1, which is likely to be less immunogenic and more readily produced than the full-length recombinant protein. Peptides and derivatives of liver fluke granulin that maintain the bioactivity represent a key advance towards identification of a novel therapies for treatment of wounds.

Experimental Section

Peptide synthesis and purification

Truncated granulin peptides were synthesised using manual solid-phase peptide synthesis using fluorenylmethyloxycarbonyl (FMOC) chemistry. Peptides were assembled on 2-chlorotrityl chloride resin (Auspep, Australia). Amino acids were activated using 2-(1H-benzotriazol-1-yl)-1,1,3,3-tetramethyluronium hexafluorophosphate (HBTU - Iris Germany) in peptide grade dimethylformamide *(*DMF -Auspep, Australia). Peptides were cleaved using a mixture of 95% TFA/2.5% TIPS/2.5% H_2O. The TFA was removed by evaporation with nitrogen and ice-cold diethyl ether was added to the residue. Ether was removed by filtration and the peptide was dissolved in 40% acetonitrile/water mixture containing 0.1% trifluoroacetic acid (TFA) and subsequently freeze-dried. The resulting crude peptides were purified with reverse phase high performance liquid chromatography (RP-HPLC) on a C-18 preparative column (Phenomenex Jupiter 10µm C_{18} 300Å 250x21.2 mm). Gradients of 1%/min of 0%-80% solvent B (90% acetonitrile in 0.045% TFA in H_2O) and solvent A (aqueous 0.045% TFA in H_2O) were used and the eluent was monitored at 215 and 280 nm. Peptides were oxidised by stirring a solution of the peptide in 100 mM ammonium bicarbonate (pH 8.2) containing 5 mM reduced glutathione and left overnight at room temperature and purified using RP-HPLC on a C-18 preparative column (Phenomenex Jupiter 10µm C_{18} 300Å 250x21.2 mm). The purity of the peptides was assessed using analytical RP-HPLC and all peptides had ≥95% purity.

To confirm the disulfide connectivity of the truncated peptides, *Ov*-GRN$_{12-34}$ was synthesised with selective protection of the cysteine residues. Cys1 and Cys14 were side-chain protected with ACM groups and Cys8 and Cys23 with (Trt) protecting groups. Following cleavage and purification of the crude peptide the disulfide bond between Cys8 and Cys23 was formed in 100 mM ammonium bicarbonate and the peptide was purified using the procedure described above. The S-ACM groups were subsequently removed by stirring 2 mg of peptide in 0.5 mL TFA, 10 uL anisole and 25 mg silver trifluoromethanesulfonate at 4°C for 1.5 h. Cold ether (10 mL) was added to the mixture and the precipitate collected by centrifugation. The precipitate was washed twice with ether and oxidized, without further purification, overnight using a solution of 50% DMSO in 0.5 M HCl. The solution was diluted 15 times with water and the fully folded peptide was purified by HPLC using 1% ACN gradient on a C-18 preparative column (Phenomenex Jupiter 10µm C_{18} 300Å 250x21.2 mm).

Auto-induction of recombinant protein expression in E. coli

Ov-grn-1 pET41a or *Escherichia coli* thioredoxin (*trx*) cDNAs contained within the pET32a (Novagen) plasmid were transfected into BL21 *E. coli* cells (Life Technologies) and used to create recombinant proteins with auto-induction as described[4, 22]. Briefly, ZYM-5052 culture media were supplemented with 100 µM Fe(III)Cl_3 and 100 µg/L kanamycin to produce recombinant protein (r*Ov*-GRN-1) or 50 µg/L ampicillin to produce TRX. Two hundred (200) ml of inoculated media in a one-litre baffled Erlenmeyer flask was incubated overnight at 37°C at 300 rpm rotation to induce expression with auto-induction.

Recombinant Protein Purification

Purification of r*Ov*-GRN-1 was achieved using an AKTA10 purification system at 4°C (GE Healthcare)[23]. The BL21 *E. coli* pellet was lysed with 3 freeze/thaw cycles followed by sonication on ice with a Q4000 unit (Qsonix). Twenty (20) g of the resulting insoluble pellet was solubilized in 400 ml urea-containing nickel binding buffer (8 M urea/300 mM NaCl/50 mM imidazole/50 mM sodium phosphate pH 8 [Sigma]) at 4°C for 24 h with slow agitation. The 0.22 µM filtered supernatant was passed over 2 × 5 ml Histrap IMAC nickel columns (GE Healthcare) and washed with increasing imidazole concentrations (two column volumes [CV] at 50 mM/5 CV at 100 mM) and eluted with 500 mM imidazole in binding buffer. The control TRX protein was expressed in the same fashion but under native conditions (without chaotropic agents) and purified with Histrap IMAC Nickel columns[23].

Protein refolding and purification

Refolding of urea-denatured r*Ov*-GRN-1 was performed with 28 mL of G10 Sephadex (GE) resin on a XK16/20 column (GE) as described[23]. A 120 ml Superdex 30 XK16/60 column (GE) was used to fractionate 3 ml of refolded r*Ov*-GRN-1 into 150 mM NaCl, 50 mM sodium phosphate, pH 6, at a flow rate of 1 ml/min. Fractions containing r*Ov*-GRN-1 monomer eluting at a size equivalent of ~1 kDa (based on the fold of granulin proteins despite a denatured molecular size of 10.4 kDa) were pooled. Protein concentration was determined by a combination of microplate Bradford assay (Biorad) and absorbance at 280 nm.

NMR spectroscopy and structure determination

Purified peptides were dissolved in 90%H_2O/10% D_2O to provide a ~0.2 mM stock. 2D ^1H-^1H TOCSY, ^1H-^1H NOESY, ^1H-^1H DQF-COSY, ^1H-^{15}N HSQC, and ^1H-^{13}C HSQC spectra were acquired at 290 K using a 600 MHz AVANCE III NMR spectrometer (Bruker, Karlsruhe, Germany) equipped with a cryogenically cooled probe. Spectra were recorded with an interscan delay of 1 s. NOESY spectra were acquired with a mixing time of 200 ms, and TOCSY spectra were acquired with an isotropic mixing period of 80 ms. All spectra were assigned using CCPNMR[24] based on the approach described by Wuthrich[25] The αH secondary shifts were determined by subtracting the random coil ^1H NMR chemical shifts of Wishart[26] from experimental αH chemical shifts.

The three-dimensional structures of *Ov*-GRN_{12-34} and *Ov*-GRN_{12-35_3s} were determined. The 2D NOESY spectra were automatically assigned and an ensemble of structures calculated using the program CYANA[27]. Torsion-angle restraints predicted using TALOS+ were used in the structure calculations. Disulfide-bond connectivities (Cys1-Cys14, Cys8-Cys23) were included in the calculations for *Ov*-GRN_{12-34} because these bonds were confirmed by selective protection of the cysteine residues. Selective protection of the cysteine residues was not used for *Ov*-GRN_{12-35_3s} in an attempt to isolate the most energetically favourable form. Consequently, the structures were calculated with the 15 possible disulfide connectivities. An analysis of the CYANA target functions was carried out to determine the most likely connectivity. Structures were visualised using MOLMOL[28].

Mammalian cell culture

The non-malignant cholangiocyte cell line H69 is a SV40-transformed human bile duct epithelial cell line derived from human liver, kindly provided by Dr. Gregory J. Gores, Mayo Clinic, Rochester, Minnesota. H69 cells[23, 29, 30] were maintained in T75cm^2 vented flasks (Corning) as monolayers as described[31] with minor modifications. Cells were maintained with regular splitting using 0.25% trypsin (Life Technologies) every 2–5 days in complete media [RPMI (Sigma) with growth factor-supplemented specialist complete media[30] [DMEM/F12 with high glucose, 10% FCS, 1×antibiotic/antimycotic, 25 µg/ml adenine, 5 µg/ml insulin, 1 µg/ml epinephrine, 8.3 µg/ml holo-transferrin, 0.62 µg/ml, hydrocortisone, 13.6 ng/ml T3 and 10 ng/ml EGF – Life Technologies]. Low nutrient media for cell proliferation assays was 5% complete media, i.e. 0.5% FCS and 1/20th of the growth factor concentrations listed above for complete media. The identities (human-derived) of the cell line were confirmed with single tandem repeat (STR) analysis in January 2015 (15/15 positive loci across 2 alleles) and mycoplasma free at the DNA Diagnostics Centre (DDC)–medical (U.S.A.), accredited/certified by CAP, ISO/IEC 17025:2005 through ACLASS.

Cell proliferation monitoring in real time using xCELLigence

Cells were seeded at 1,500 cells/well in 180 µl complete media (above) in E-plates (ACEA Biosciences) and grown overnight while monitored with an xCELLigence SP system (ACEA Biosciences) which monitors cellular events in real time by measuring electrical impedance across interdigitated gold micro-electrodes integrated into the base of tissue culture plates[32]. Cells were washed three times with PBS prior to addition of 180 µl of low nutrient media (above) and incubated for a minimum of 6 h before further treatment. Treatments were prepared at 10× concentration and added to each well in a total volume of 20 µl. The xCELLigence system

recorded cell indexes at intervals of one hour for 5-6 days following treatment. Readings for the cell index were normalized prior to treatment and cell proliferation ratios represent the relative numbers of cells compared to control cells at day 4. Dose response curves for each peptide were generated from 3-6 independent experiments each with 4-6 replicates. Comparisons of induction of cell proliferation in response to treatments were accomplished using two-way ANOVA test with Dunnett's multiple comparison correction, using GraphPad Prism 6.02.

Mouse wounding assay

These studies were conducted with the approval of the James Cook University Small Animal Ethics Committee, applications A1806 and A2204, as described[6]. Briefly, female 11-12 week old BALB/c mice weighing 19-23 g were sourced from the Australian ARC (Animal Resources Centre) and randomly allocated into groups of 4-5 mice. Mice were anesthetized (intraperitoneal xylazine 16 mg/kg; ketamine 80 mg/kg), after which a skin-deep wound on the crown of the head was inflicted using a 5 mm biopsy punch (Zivic instruments). Betadine liquid antiseptic (Sanofi) was applied followed by application of 50 µl that contained either 71 pmoles of Regranex (treatment of 71 pmoles equals 1 µg per 0.25 cm^2 wound, as recommended by manufacturer Smith and Nephew), 56 pmoles of r*Ov*-GRN-1, *Ov*-GRN-1 peptides, control peptide (EADRKYDEVARKLAMVEADL), TRX or PBS suspended in 1.5% methylcellulose (Sigma). Wounds were photographed daily and after blinding treatment groups the area of the lesion was measured with ImageJ software and plotted as percent of wound closure from original wound images. Wound healing rates were compared with two-way ANOVA test with Dunnett's correction for multiple comparisons, using GraphPad prism 6.02. Each mouse wounding study was conducted at least twice to provide reproducibility.

Acknowledgements

Funding: This research was supported by an R01 grant from the National Cancer Institute, U.S.A (R01CA164719) and a program grant from National Health and Medical Research Council, Australia (NHMRC) (1037304). Fellowship support was provided to AL from NHMRC (1020114) and NLD from the Australian Research Council (FF110100226). The content is solely the responsibility of the authors and does not necessarily represent the official views of the NCI or NIH. The funders had no role in study design, data collection and analysis, decision to publish, or preparation of the manuscript.

The PDB ID codes are 5UJH and 5UJG for *Ov*-GRN$_{12\text{-}34}$ and *Ov*-GRN$_{12\text{-}35_3s}$ respectively. Authors will release the atomics coordinates and experimental data upon article publication.

Supporting Information.

Structure statistics for *Ov*-GRN$_{12\text{-}34}$ and *Ov*-GRN$_{12\text{-}35_3s}$. Chemical shift analysis of carp granulin-1. Analysis of different disulfide connectivities for *Ov*-GRN$_{12\text{-}35_3s}$. Wound healing photos.

Author Information

Corresponding Authors

*Email norelle.daly@jcu.edu.au. Tel: +61 7 4232 1815

*Email alex.loukas@jcu.edu.au. Tel: +61 7 4232 1608

Abbreviations Used

FMOC, Fluorenymethyloxycarbonyl; *Ov*-GRN, *Opisthorchis viverrine* granulin*;* PBS, phosphate buffered saline; PGRN, progranulin, TRX, thioredoxin.

References

1. He, Z.; Ong, C. H.; Halper, J.; Bateman, A. Progranulin is a mediator of the wound response. *Nat. Med.* **2003**, *9*, 225-229.
2. Mulvenna, J.; Sripa, B.; Brindley, P. J.; Gorman, J.; Jones, M. K.; Colgrave, M. L.; Jones, A.; Nawaratna, S.; Laha, T.; Suttiprapa, S.; Smout, M. J.; Loukas, A. The secreted and surface proteomes of the adult stage of the carcinogenic human liver fluke *Opisthorchis viverrini*. *Proteomics.* **2010**, *10*, 1063-1078.
3. Laha, T.; Pinlaor, P.; Mulvenna, J.; Sripa, B.; Sripa, M.; Smout, M. J.; Gasser, R. B.; Brindley, P. J.; Loukas, A. Gene discovery for the carcinogenic human liver fluke, *Opisthorchis viverrini*. *BMC Genomics.* **2007**, *8*, 189.
4. Smout, M. J.; Laha, T.; Mulvenna, J.; Sripa, B.; Suttiprapa, S.; Jones, A.; Brindley, P. J.; Loukas, A. A granulin-like growth factor secreted by the carcinogenic liver fluke, *Opisthorchis viverrini*, promotes proliferation of host cells. *PLoS Pathog.* **2009**, *5*, e1000611.
5. Smout, M. J.; Sripa, B.; Laha, T.; Mulvenna, J.; Gasser, R. B.; Young, N. D.; Bethony, J. M.; Brindley, P. J.; Loukas, A. Infection with the carcinogenic human liver fluke, *Opisthorchis viverrini*. *Mol. Biosyst.* **2011**, *7*, 1367-1375.
6. Smout, M. J.; Sotillo, J.; Laha, T.; Papatpremsiri, A.; Rinaldi, G.; Pimenta, R. N.; Chan, L. Y.; Johnson, M. S.; Turnbull, L.; Whitchurch, C. B.; Giacomin, P. R.; Moran, C. S.; Golledge, J.; Daly, N.; Sripa, B.; Mulvenna, J. P.; Brindley, P. J.; Loukas, A. Carcinogenic parasite secretes growth factor that accelerates wound healing and potentially promotes neoplasia. *PLoS Pathog.* **2015**, *11*, e1005209.
7. Hrabal, R.; Chen, Z.; James, S.; Bennett, H. P.; Ni, F. The hairpin stack fold, a novel protein architecture for a new family of protein growth factors. *Nat. Struct. Biol.* **1996**, *3*, 747-752.
8. Ong, C. H.; Bateman, A. Progranulin (granulin-epithelin precursor, PC-cell derived growth factor, acrogranin) in proliferation and tumorigenesis. *Histol. Histopathol.* **2003**, *18*, 1275-1288.
9. Tolkatchev, D.; Malik, S.; Vinogradova, A.; Wang, P.; Chen, Z.; Xu, P.; Bennett, H. P.; Bateman, A.; Ni, F. Structure dissection of human progranulin identifies well-folded granulin/epithelin modules with unique functional activities. *Protein Sci.* **2008**, *17*, 711-724.
10. Alquezar, C.; de la Encarnacion, A.; Moreno, F.; Lopez de Munain, A.; Martin-Requero, A. Progranulin deficiency induces overactivation of WNT5A expression via TNF-alpha/NF-kappaB pathway in peripheral cells from frontotemporal dementia-linked granulin mutation carriers. *J. Psychiatry Neurosci.* **2016**, *41*, 225-239.
11. Park, B.; Buti, L.; Lee, S.; Matsuwaki, T.; Spooner, E.; Brinkmann, M. M.; Nishihara, M.; Ploegh, H. L. Granulin is a soluble cofactor for toll-like receptor 9 signaling. *Immunity.* **2011**, *34*, 505-513.

12. Yeh, J. E.; Kreimer, S.; Walker, S. R.; Emori, M. M.; Krystal, H.; Richardson, A.; Ivanov, A. R.; Frank, D. A. Granulin, a novel STAT3-interacting protein, enhances STAT3 transcriptional function and correlates with poorer prognosis in breast cancer. *Genes Cancer.* **2015**, *6*, 153-168.
13. Yip, C. W.; Cheung, P. F.; Leung, I. C.; Wong, N. C.; Cheng, C. K.; Fan, S. T.; Cheung, S. T. Granulin-epithelin precursor interacts with heparan sulfate on liver cancer cells. *Carcinogenesis.* **2014**, *35*, 2485-2494.
14. Vranken, W. F.; Chen, Z. G.; Xu, P.; James, S.; Bennett, H. P.; Ni, F. A 30-residue fragment of the carp granulin-1 protein folds into a stack of two beta-hairpins similar to that found in the native protein. *J. Pept. Res.* **1999**, *53*, 590-597.
15. Tolkatchev, D.; Ng, A.; Vranken, W.; Ni, F. Design and solution structure of a well-folded stack of two beta-hairpins based on the amino-terminal fragment of human granulin A. *Biochemistry.* **2000**, *39*, 2878-2886.
16. Wishart, D. S.; Bigam, C. G.; Holm, A.; Hodges, R. S.; Sykes, B. D. ^{1}H, ^{13}C and ^{15}N random coil NMR chemical shifts of the common amino acids. I. Investigations of nearest-neighbor effects. *J. Biomol. NMR.* **1995**, *5*, 67-81.
17. Saether, O.; Craik, D. J.; Campbell, I. D.; Sletten, K.; Juul, J.; Norman, D. G. Elucidation of the primary and three-dimensional structure of the uterotonic polypeptide kalata B1. *Biochemistry.* **1995**, *34*, 4147-4158.
18. Daly, N. L.; Koltay, A.; Gustafson, K., R.; Boyd, M. R.; Casas-Finet, J. R.; Craik, D. J. Solution structure by NMR of circulin A: a macrocyclic knotted peptide having anti-HIV activity. *J. Mol. Biol.* **1999**, *285*, 333-345.
19. Chen, X.; Chang, J.; Deng, Q.; Xu, J.; Nguyen, T. A.; Martens, L. H.; Cenik, B.; Taylor, G.; Hudson, K. F.; Chung, J.; Yu, K.; Yu, P.; Herz, J.; Farese, R. V., Jr.; Kukar, T.; Tansey, M. G. Progranulin does not bind tumor necrosis factor (TNF) receptors and is not a direct regulator of TNF-dependent signaling or bioactivity in immune or neuronal cells. *J. Neurosci.* **2013**, *33*, 9202-9213.
20. Etemadi, N.; Webb, A.; Bankovacki, A.; Silke, J.; Nachbur, U. Progranulin does not inhibit TNF and lymphotoxin-alpha signalling through TNF receptor 1. *Immunol. Cell Biol.* **2013**, *91*, 661-664.
21. Rollinson, S.; Young, K.; Bennion-Callister, J.; Pickering-Brown, S. M. Identification of biological pathways regulated by PGRN and GRN peptide treatments using transcriptome analysis. *Eur. J. Neurosci.* **2016**, *44*, 2214-2225.
22. Studier, F. W. Protein production by auto-induction in high density shaking cultures. *Protein Expr. Purif.* **2005**, *41*, 207-234.
23. Smout, M. J.; Mulvenna, J. P.; Jones, M. K.; Loukas, A. Expression, refolding and purification of *Ov*-GRN-1, a granulin-like growth factor from the carcinogenic liver fluke, that causes proliferation of mammalian host cells. *Protein Expr. Purif.* **2011**, *79*, 263-270.
24. Vranken, W. F.; Boucher, W.; Stevens, T. J.; Fogh, R. H.; Pajon, A.; Llinas, M.; Ulrich, E. L.; Markley, J. L.; Ionides, J.; Laue, E. D. The CCPN data model for NMR spectroscopy: development of a software pipeline. *Proteins.* **2005**, *59*, 687-696.
25. Wüthrich, K. (1986). *NMR of proteins and nucleic acids*, Wiley-Interscience, New York.
26. Wishart, D. S.; Bigam, C. G.; Yao, J.; Abildgaard, F.; Dyson, H. J.; Oldfield, E.; Markley, J. L.; Sykes, B. D. 1H, 13C and 15N chemical shift referencing in biomolecular NMR. *J. Biomol. NMR.* **1995**, *6*, 135-140.

27. Guntert, P. Automated NMR structure calculation with CYANA. *Methods Mol. Biol.* **2004**, *278*, 353-378.
28. Koradi, R.; Billeter, M.; Wüthrich, K. MOLMOL: a program for display and analysis of macromolecular structures. *J. Mol. Graph.* **1996**, *14*, 29-32.
29. Grubman, S. A.; Perrone, R. D.; Lee, D. W.; Murray, S. L.; Rogers, L. C.; Wolkoff, L. I.; Mulberg, A. E.; Cherington, V.; Jefferson, D. M. Regulation of intracellular pH by immortalized human intrahepatic biliary epithelial cell lines. *Am. J. Physiol.* **1994**, *266*, G1060-1070.
30. Matsumura, T.; Takesue, M.; Westerman, K. A.; Okitsu, T.; Sakaguchi, M.; Fukazawa, T.; Totsugawa, T.; Noguchi, H.; Yamamoto, S.; Stolz, D. B.; Tanaka, N.; Leboulch, P.; Kobayashi, N. Establishment of an immortalized human-liver endothelial cell line with SV40T and hTERT. *Transplantation.* **2004**, *77*, 1357-1365.
31. Papatpremsiri, A.; Smout, M. J.; Loukas, A.; Brindley, P. J.; Sripa, B.; Laha, T. Suppression of *Ov*-grn-1 encoding granulin of *Opisthorchis viverrini* inhibits proliferation of biliary epithelial cells. *Exp. Parasitol.* **2015**, *148*, 17-23.
32. Xing, J. Z.; Zhu, L.; Jackson, J. A.; Gabos, S.; Sun, X. J.; Wang, X. B.; Xu, X. Dynamic monitoring of cytotoxicity on microelectronic sensors. *Chem. Res. Toxicol.* **2005**, *18*, 154-161.

Figures

Figure 1

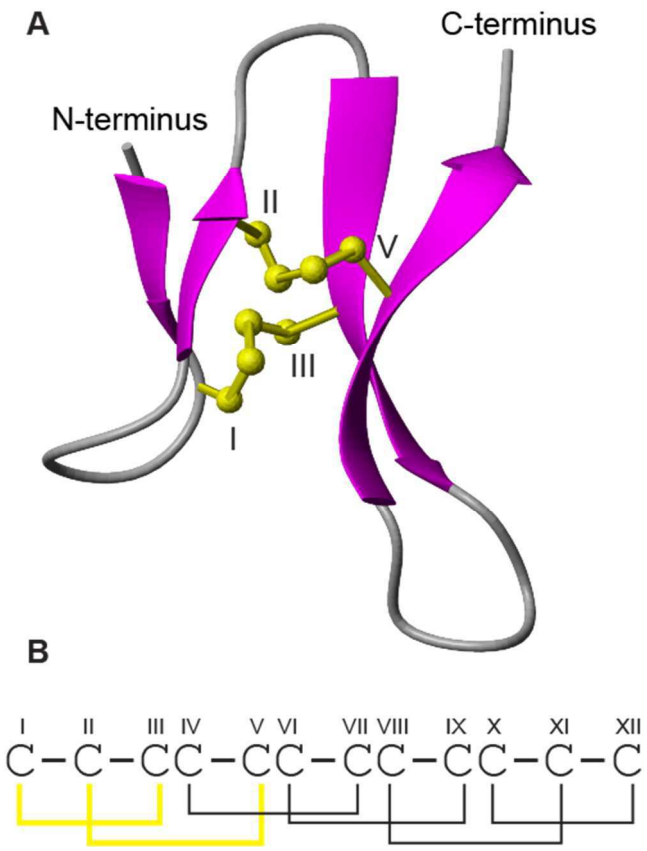

Figure 2

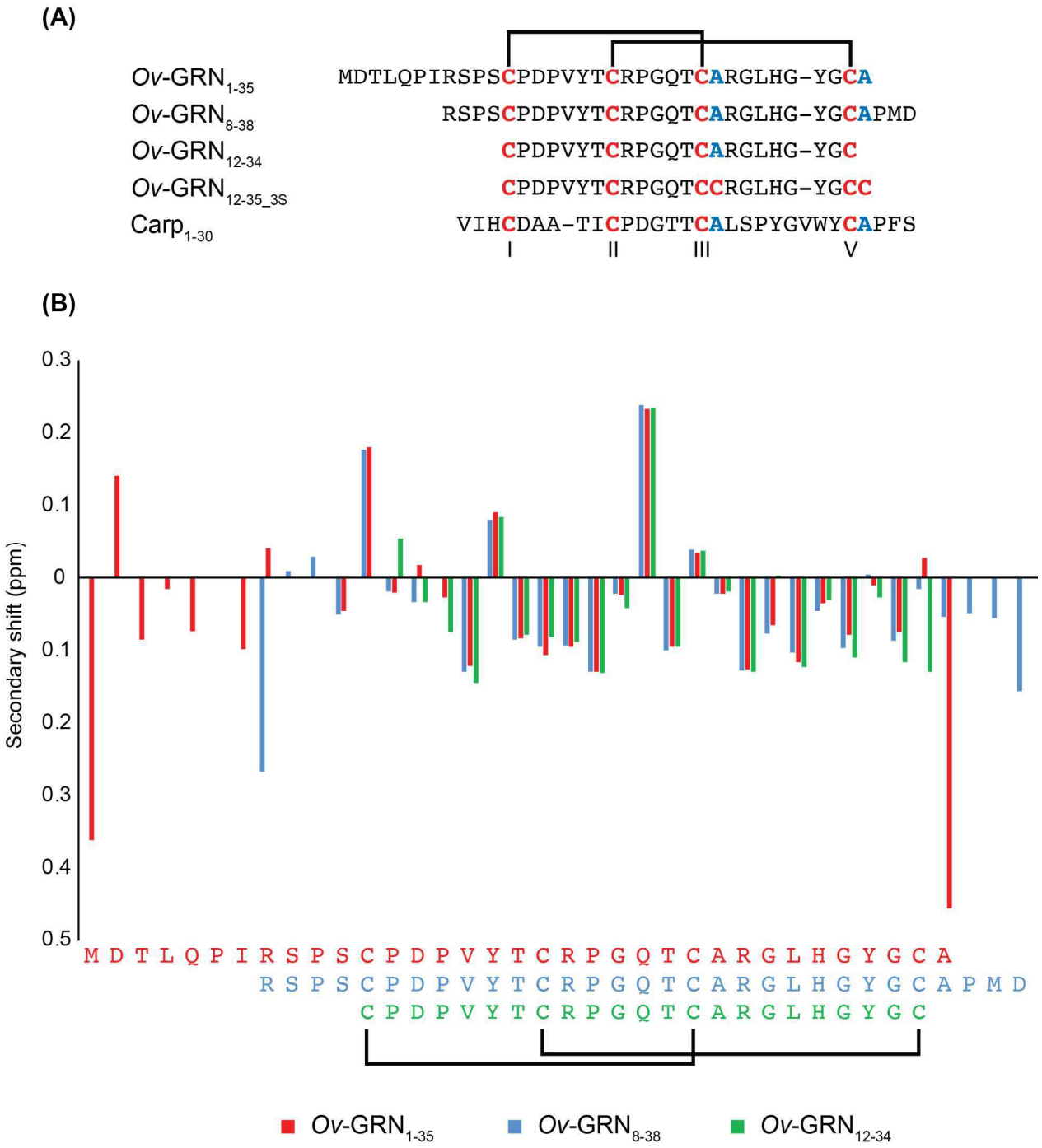
(A)
Ov-GRN1-35 MDTLQPIRSPSCPDPVYTCRPGQTCARGLHG-YGCA
Ov-GRN8-38 RSPSCPDPVYTCRPGQTCARGLHG-YGCAPMD
Ov-GRN12-34 CPDPVYTCRPGQTCARGLHG-YGC
Ov-GRN12-35_3S CPDPVYTCRPGQTCCRGLHG-YGCC
Carp1-30 VIHCDAA-TICPDGTTCALSPYGVWYCAPFS
I II III V
(B)
Secondary shift (ppm)
0.3 0.2 0.1 0 0.1 0.2 0.3 0.4 0.5
M D T L Q P I R S P S C P D P V Y T C R P G Q T C A R G L H G Y G C A
R S P S C P D P V Y T C R P G Q T C A R G L H G Y G C A P M D
C P D P V Y T C R P G Q T C A R G L H G Y G C
Ov-GRN1-35 Ov-GRN8-38 Ov-GRN12-34

Figure 3

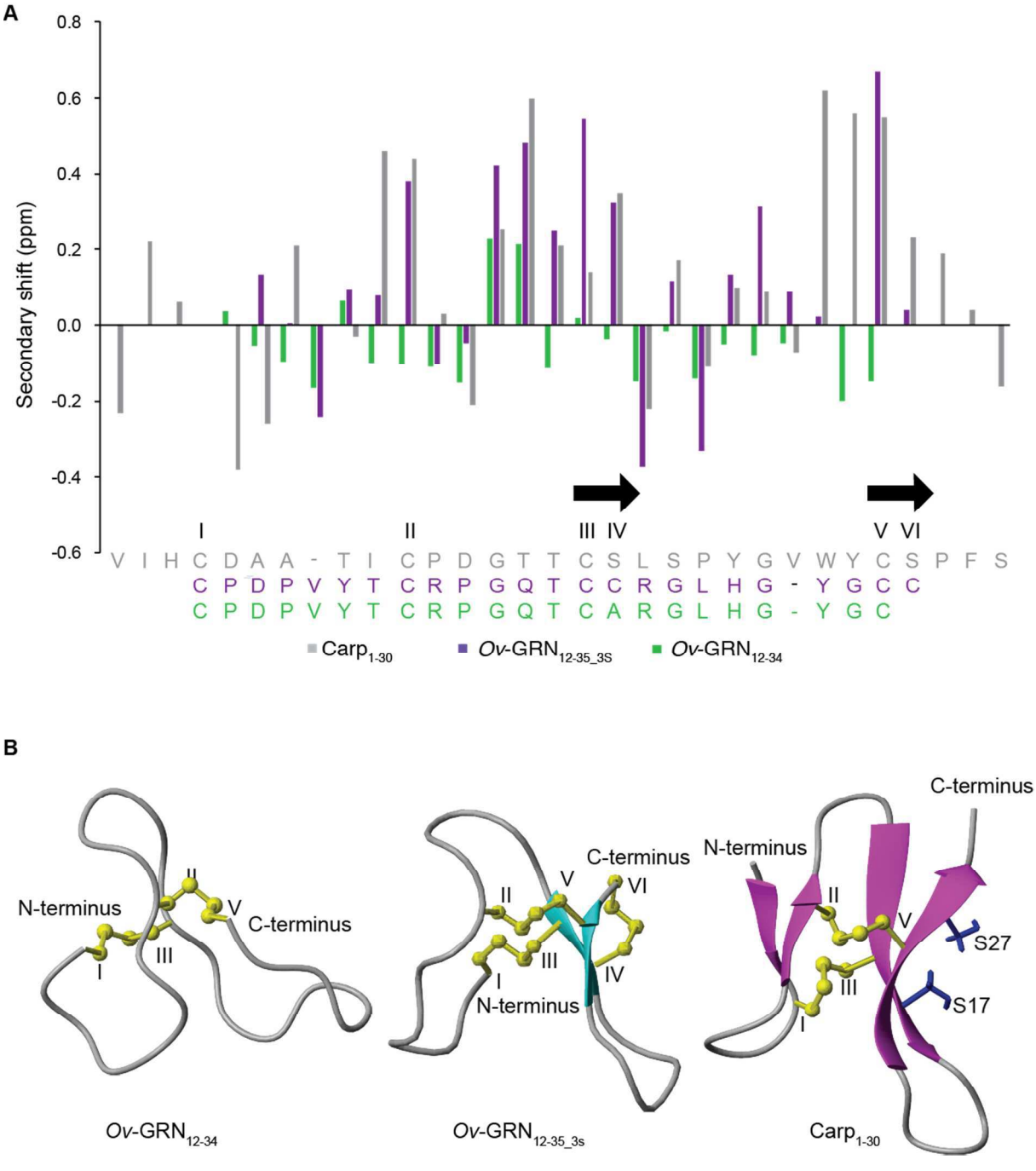
A
Secondary shift (ppm)
0.8
0.6
0.4
0.2
0.0
-0.2
-0.4
-0.6
I
II
III IV
V VI
V I H C D A A - T I C P D G T T C S L S P Y G V W Y C S P F S
C P D P V Y T C R P G Q T C C R G L H G - Y G C C
C P D P V Y T C R P G Q T C A R G L H G - Y G C
Carp1-30
Ov-GRN12-35_3S
Ov-GRN12-34
B
N-terminus
C-terminus
I
II
III
V
Ov-GRN12-34
C-terminus
N-terminus
I
II
III
IV
V
VI
Ov-GRN12-35_3s
C-terminus
N-terminus
I
II
III
V
S27
S17
Carp1-30

Figure 4

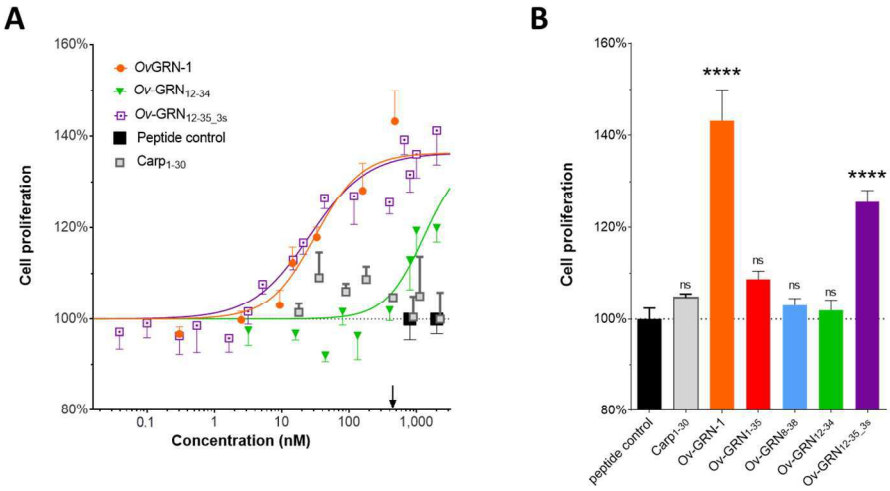
A
160%
140%
120%
100%
80%
Cell proliferation
OvGRN-1
Ov GRN12-34
Ov-GRN12-35_3s
Peptide control
Carp1-30
0.1
1
10
100
1,000
Concentration (nM)
B
160%
140%
120%
100%
80%
Cell proliferation
****
****
ns
ns
ns
ns
peptide control
Carp1-30
Ov-GRN-1
Ov-GRN1-35
Ov-GRN8-38
Ov-GRN12-34
Ov-GRN12-35_3s

Figure 5

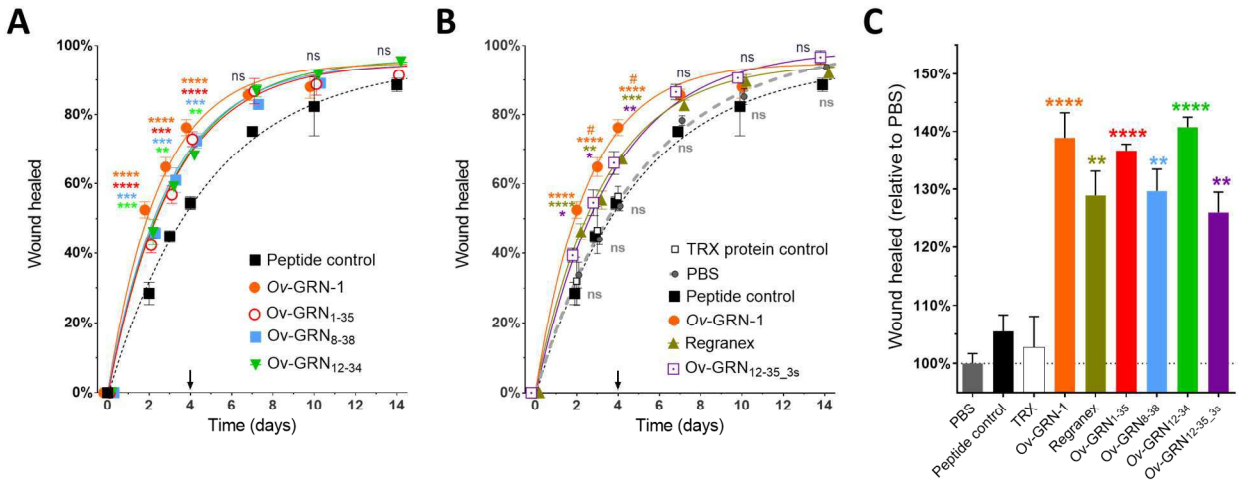
A
Wound healed
Time (days)
Peptide control
Ov-GRN-1
Ov-GRN1-35
Ov-GRN8-38
Ov-GRN12-34
B
Wound healed
Time (days)
TRX protein control
PBS
Peptide control
Ov-GRN-1
Regranex
Ov-GRN12-35_3s
C
Wound healed (relative to PBS)
PBS
Peptide control
TRX
Ov-GRN-1
Regranex
Ov-GRN1-35
Ov-GRN8-38
Ov-GRN12-34
Ov-GRN12-35_3s

Figure Legends

Figure 1. Three-dimensional structure of a 30 residue N-terminal domain of carp granulin-1. (A) PDB code 1QGM, the β-strands are shown as purple arrows and the disulfide bonds in yellow ball and stick format. The image was generated using MolMol. (B) The disulfide connectivity in the full length carp granulin-1 protein[7]. Cysteines are designated with sequential roman numerals I-XII. The two bonds in the truncated carp granulin-1 are highlighted in yellow.

Figure 2. Sequences and secondary shifts of the *Ov*-GRN-1 truncated analogues. (A) Sequences show CysIV and CysVI were replaced with alanine residues; the cysteines are highlighted in red and the substitutions are shown in blue. The N-terminal 30 residues of carp granulin-1 is also provided, with CysIV and VI replaced with alanine residues. (B) Secondary shifts of *Ov*-GRN-1 peptides with four cysteine residues (*Ov*-GRN_{1-35}, *Ov*-GRN_{8-38} and *Ov*-GRN_{12-34}). The secondary shifts were derived by subtracting random coil shifts[16] from the αH shifts. The similarity in the secondary shifts for the conserved residues indicates that the overall fold is the same in the three peptides. Color scheme is retained in Figures 2-5. Both panels: black connecting lines represent disulfide bond connectivity.

Figure 3: Structural analysis of *Ov*-GRN_{12-34} and *Ov*-GRN_{12-35_3s}. (A) Secondary shifts of *Ov*-GRN_{12-34} and *Ov*-GRN_{12-35_3s} compared to carp $granulin_{1-30}$. The secondary shifts were derived by subtracting random coil shifts[16] from the αH shifts. *Ov*-GRN_{12-34} has significantly different secondary shifts compared to *Ov*-GRN_{12-35_3s} and $carp_{1-30}$, and lacks positive shifts indicating a

lack of β-sheet structure. Despite the differences in sequence the trends for the secondary shifts between *Ov*-GRN$_{12\text{-}35_3s}$ and carp$_{1\text{-}30}$ are similar indicating that the β-sheet present in carp granulin-1 is also present in *Ov*-GRN$_{12\text{-}35_3s}$ (black arrows). (B) The structures of *Ov*-GRN$_{12\text{-}34}$ and *Ov*-GRN$_{12\text{-}35_3s}$ were determined using NMR spectroscopy and confirms that *Ov*-GRN$_{12\text{-}34}$ does not contain β-sheet structure but Ov-GRN$_{12\text{-}35_3s}$ does (blue arrows). Disulfide bonds are shown as yellow ball and stick representations and the structure of carp$_{1\text{-}30}$ are shown for comparison. The side-chains of residues Ser17 and Ser27 are highlighted on the carp$_{1\text{-}30}$ structure, to indicate the Cys-Ser substituted sites of CysIV and Cys VI. Based on this structure it appears likely that CysIV and CysVI of carp$_{1\text{-}30}$ could form a disulfide bond, consistent with the likely connectivity in *Ov*-GRN$_{12\text{-}35_3s}$.

Figure 4. Liver fluke granulin peptides induce cell proliferation. (A) *Opisthorchis viverrini* granulin peptides but not carp granulin$_{1\text{-}30}$ induced proliferation of H69 human cholangiocytes at a range of concentrations as monitored using xCELLigence. Only selected treatments are graphed to aid visualization. Variable slope dose response lines of best fit show proliferation four days after a single application of treatment. *Ov*-GRN$_{12\text{-}35_3s}$ potency characterized by significantly increased cell proliferation observed at final concentrations of ≥15 nM ($p<0.05$). Black arrow denotes 400-483 nM concentration used in panel B. (B) Mean proliferation at 400 nM of all *Ov*-GRN-1 synthesized peptides and 483 nM *Ov*-GRN-1 protein from panel A. ns = not significant, ****$p<0.0001$. Both Panels: 2-way ANOVA test with Dunnett's correction for multiple comparisons was used to compare treatments with relevant treatment controls (*Ov*-GRN-1 protein relative to thioredoxin expression matched recombinant protein control and peptides relative to

peptide control (20-residue peptide derived from tropomyosin). Mean values from 4-6 replicates pooled from 2-4 experiments with SEM bars shown either above or below for clarity.

Figure 5. Mouse wound healing activity of *Ov*-GRN-1 and peptides. (A+B) Wound healing outcomes from treatments with 56 pmoles of recombinant *Ov*-GRN-1, *Ov*-GRN-1 peptides, unrelated peptide, thioredoxin (TRX) protein controls and 71 pmoles Regranex in 1.5% methylcellulose gel applied daily in 50 µl volume from days 0-4 to a ~0.2 cm^2 wound arising from biopsy punch to the scalp between the ears. To aid visualisation, data were split across two graphs with the *Ov*-GRN-1 and peptide control groups shown in both panels. No significant differences between the unrelated peptide control, PBS, or TRX protein control were noted at any time point. Black arrows denote the day 4 time point used in panel C. (C) Wound healing relative to PBS vehicle control from day 4. All panels: mean healing rates of 2-6 biological replicates of groups of 4-5 animals plotted with SEM bars. Groups have been marginally shifted left or right to aid viewing. Repeated measure 2-way ANOVA test with Dunnett's correction for multiple comparisons compare each group against each other group. Significance against peptide/protein control signified by **** = $p<0.0001$, *** = $p<0.001$, ** = $p<0.01$, * = $p<0.05$, ns=not significant. Significant treatments against Regranex signified by # = $p<0.05$. Color of asterisk or hash represents the relevant group. The colors and symbols are maintained across Figures 2-5.

Table of Contents Graphic

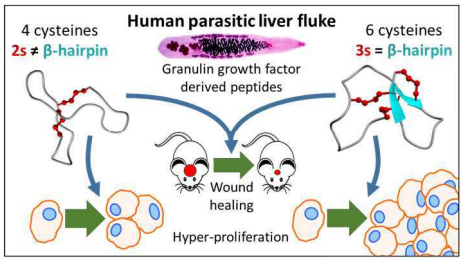

Keywords

Growth factor

Diabetes

Chronic wounds

Peptide

Granulin

Wound healing

Cell proliferation